JAAS

RSC Publishing

PAPER

View Article Online
View Journal | View Issue

Cite this: *J. Anal. At. Spectrom.*, 2013, **28**, 1068

Reassessment of relative oxide formation rates and molecular interferences on *in situ* lutetium–hafnium analysis with laser ablation MC-ICP-MS†

Justin L. Payne,*[a] Norman J. Pearson,[b] Kevin J. Grant[b] and Galen P. Halverson[ac]

A series of Hf and rare earth element (REE) solutions and glass beads have been produced in order to assess the influence of isobaric and molecular interferences on LA-MC-ICP-MS analysis of Lu–Hf isotopes in zircon. We demonstrate the capability to accurately correct for isobaric interferences of ^{176}Yb on ^{176}Hf at levels up to ^{176}Yb/^{177}Hf = 0.6 in solution mode. When using laser ablation sample introduction and REE–Hf doped glass beads we are able to accurately correct for ^{176}Yb interferences up to ^{176}Yb/^{177}Hf = 0.15. These thresholds exceed the ^{176}Yb/^{177}Hf ratios in most natural zircon and demonstrate the general robustness of the method. Unlike solution analysis, at extreme Yb interference levels (^{176}Yb/^{177}Hf ≈ 0.8) there appears to be a slight over-correction of Yb interferences. We demonstrate using theoretical calculations that for high-REE zircons, even modest oxide formation rates can lead to inaccurate ^{176}Hf/^{177}Hf ratios. This finding is confirmed by data collected on REE-doped glass beads and a natural zircon sample. Importantly, Gd oxides dominate over Dy oxides as a source of molecular interferences on Hf isotope data because Gd is more prone to oxide formation. Oxide formation rates vary depending upon sample introduction, instrument tuning and N_2 addition (in laser mode). Correction for molecular interferences is possible using a dynamic analysis routine but requires measurement of the relative Gd and Hf oxide formation rates for the analysis session. Hence the daily monitoring of Gd and Hf oxide formation rates will improve the accuracy of Lu–Hf LA-MC-ICP-MS results for high-REE/Hf zircons.

Received 18th March 2013
Accepted 3rd May 2013

DOI: 10.1039/c3ja50090j

www.rsc.org/jaas

Introduction

A challenge to accurate and precise isotope ratio measurements by laser ablation multiple-collector inductively coupled plasma mass spectrometry (LA-MC-ICP-MS) is the presence of isobaric and molecular interferences on masses of interest.[1–3] This limitation is significant during *in situ* radiogenic isotope analysis, in particular for Lu–Hf isotopic analysis of zircon. ^{176}Lu decays through β-decay to ^{176}Hf with ^{176}Hf/^{177}Hf and ^{176}Lu/^{177}Hf measured and reported in geological studies. In LA-MC-ICP-MS analysis there are two isobaric interferences on ^{176}Hf:^{176}Lu and ^{176}Yb. ^{176}Yb is the more significant and a number of different data reduction techniques are applied to correct for this interference, the two most common[4,5] of which are described below.

The first method (Method 1) uses a mass fractionation factor calculated from measurement of two interference-free Yb isotopes (either ^{171}Yb/^{173}Yb or ^{172}Yb/^{173}Yb) to calculate the intensity of the interfering ^{176}Yb signal (*e.g.* ref. 3 and 6). This approach is limited by the accuracy to which the stable isotopic ratios of Yb are known (a range is present in the literature, *e.g.* ref. 1, 7 and 8) and the statistical limitations of calculating fractionation factors on low intensity signals in the case of low-REE zircon. The second method (Method 2) involves measuring the mass fractionation factor for Hf (typically done on ^{179}Hf/^{177}Hf) and using this factor to calculate the intensity of ^{176}Yb using a modified ^{172}Yb/^{176}Yb or ^{173}Yb/^{176}Yb ratio.[2] This modified ^{17X}Yb/^{176}Yb ratio is determined by doping a standard Hf solution with different amounts of Yb and iteratively solving or using standard addition to solve for a Yb ratio that reproduces the ^{176}Hf/^{177}Hf ratio of the pure Hf standard solution. This method assumes a constant fractionation relationship between Hf and Yb and also assumes that values obtained *via* solution analysis are valid for laser ablation analysis.

The direct measurement of a Yb fractionation factor for each analysis is preferred in many studies as it removes the potential for error generated through inconsistent mass bias relationships between Hf and Yb.[1,3,9] However, in situations where a low Yb signal is obtained the large uncertainty on the

[a]*Centre for Tectonics, Resources and Exploration (TRAX), School of Earth and Environmental Sciences, University of Adelaide, SA 5005, Australia. E-mail: justin.payne@adelaide.edu.au*

[b]*ARC Centre of Excellence for Core to Crust Fluid Systems (CCFS), Department of Earth and Planetary Sciences, Macquarie University, NSW 2109, Australia*

[c]*Department of Earth and Planetary Sciences/GEOTOP, McGill University, 3450 University Street, Montreal, Quebec H3A 0E8, Canada*

† Electronic supplementary information (ESI) available. See DOI: 10.1039/c3ja50090j

Table 1 Isotope proportions (in %, IUPAC values) and potential interferences on Hf isotopes

Mass	171	172	173	175	176	177	178	179	180
Hf					5.26	18.60	27.28	13.62	35.08
Lu				97.42	2.58				
Yb	14.28	21.83	16.13		12.76				
Dy + ^{16}O[a]					*2.34*	*18.91*	*25.51*	*24.90*	*28.19*
Tb + ^{16}O				*100*					
Gd + ^{16}O	*14.80*	*20.47*	*15.65*		*21.86*				

[a] Molecular interferences are given in italics and assume oxygen composition is purely ^{16}O.

measured Yb fractionation factor outweighs the potential for errors generated by inconsistent mass bias relationships between Yb and Hf.[9]

Fisher *et al.*[4] recently addressed the assumption of similarity between solution and laser ablation mass bias relationships (*i.e.* Method 2) and suggested that the mass bias relationship is not consistent between the two sample introduction methods. This contrasts with other studies which show long term consistency between the two sample introduction methods,[5] hence there remains some uncertainty over the applicability of findings obtained on a given instrument to other instruments and operating conditions.

In addition to the well documented isobaric interferences, oxide formation, namely REE-oxides, may generate molecular interferences that affect the Hf isotope system. Oxides of Gd, Dy and Er create interferences on ^{176}Hf, ^{177}Hf, ^{178}Hf, ^{179}Hf and ^{180}Hf (Table 1). These interferences are generally considered insignificant and hence no correction is made for them. However, for high REE zircons this may not be the case. Unlike Yb and Lu isobaric interferences, the interference effects will not necessarily produce a simple linear relationship between Yb or Lu content and corrected $^{176}Hf/^{177}Hf$. Oxides of Gd, Dy and Tb also create interferences on ^{171}Yb, ^{172}Yb, ^{173}Yb and ^{175}Lu. If these interferences are significant but unaccounted for, they may affect the accuracy of the isobaric Yb and Lu interference corrections. Hawkesworth and Kemp[10] observed the influence of REE-oxides on Hf, which they attributed to the production of Dy oxide, and used N_2 addition down-stream of the ablation cell to reduce oxide formation and circumvent this issue. As the monitoring of oxide production is not routinely undertaken and/or reported in the geological literature for LA-MC-ICP-MS Lu–Hf data it is not possible to assess the potential extent of oxide-based molecular interferences on any given dataset.

In this article we make two primary contributions to the issue of interference correction in LA-MC-ICPMS measurements of the Lu–Hf isotope system. The first contribution is the theoretical calculation of the nature and extent of molecular interferences for differing oxide formation rates and differing REE concentrations and patterns. We then assess the effects of isobaric and molecular interferences in a series of natural zircon and synthetic glass beads to redress the perceived lack of importance of molecular interferences in LA-MC-ICP-MS Hf isotope measurements. We propose a correction protocol for these molecular interferences.

Analytical methods

The experimental component of this study consisted of a series of measurements targeted at testing the relationship and viability of interference corrected Hf isotope measurements *via* solution and laser ablation. Unless otherwise noted, measurements were conducted at a joint University of Adelaide and Commonwealth Scientific and Industry Research Organisation (CSIRO) facility (Adelaide, South Australia) using a Thermo-Electron Neptune MC-ICP-MS coupled to either a New Wave UP-193 Excimer laser or an ESI Apex desolvating nebuliser for solution mode. Additional measurements of relative oxide formation rates and AMES Hf metal composition were conducted at Macquarie University, Australia, using a Nu Instruments MC-ICP-MS coupled to a Nu Instruments Desolvating Nebuliser (DSN). Relative oxide formation rates were also measured using an Agilent 7500cs ICP-MS ('wet' solution sample introduction) at Macquarie University.

Solution analyses to assess isobaric interference correction involved the measurement of a pure Hf isotope standard JMC475 solution and a series of 100 ppb JMC475 solutions spiked with Yb (1000 ppm Yb ACR standard (NIST TRACEABLE)) to provide concentrations ranging from 5 ppb to 50 ppb. To assess molecular/oxide interference corrections, a series of 100 ppb JMC475 solutions were spiked with varying concentrations of Gd (0.67 ppb to 5.72 ppb), Dy (2.68 ppb to 21.78 ppb) and Tb (0.247 ppb to 1.98 ppb). The relative concentrations of these REEs are representative of typical concentrations found in natural zircon.

Equivalent measurements for laser ablation were obtained by producing a series of glass beads (Diopside (75%) – Forsterite (25%) starting composition) spiked with 1 wt% Hf (JMC475). Glass beads were produced following procedures similar to those described in O'Neill[11] and Grant and Wood.[12] To assess isobaric interferences, glass beads were produced containing Hf and 0–10 000 ppm Yb (1000 ppm Yb ACR standard). To assess molecular interferences, two series of glass beads were produced with a nominal content of 1 wt% Hf (JMC475) and varying levels of Dy or Gd (up to 1000 ppm) and a glass bead with a REE composition equivalent to a REE-enriched zircon (containing 1 wt% Hf, 304 ppm Lu, 1589 ppm Yb, 589 ppm Er, 248 ppm Dy, 20 ppm Tb and 48 ppm Gd). Because it is not possible to directly measure the REE oxide formation rates in natural samples it is necessary to establish the relative oxide formation rates of Hf and Gd, Dy and Er. This was done with a series of oxide formation measurements on single element

solutions or glass beads of Hf, Gd, Dy, Er and Yb over the course of the analytical session/s.

Solution analyses were primarily made using the H-cone skimmer cone. For pure Hf standard solutions and Yb-doped Hf solutions, ^{171}Yb, ^{173}Yb, ^{175}Lu, ^{176}Hf(+Lu + Yb), ^{177}Hf, ^{178}Hf, ^{179}Hf and ^{180}Hf were measured in Faraday cups (Table 2) with 10^{-11} Ω amplifiers. Amplifier rotation was not used as it is not suitable during laser ablation analysis. Solutions were analysed using a routine that included a pre-analysis peak centre and baseline measurement followed by 7 blocks of 20 integrations with an integration time of 4.194 seconds (total time = 587 s). Solution analysis of Yb-doped Hf solutions was also conducted using the X-cone skimmer cone. This was done to replicate the configuration used during laser ablation analysis, during which the X-cone is used to maximise sensitivity. Measurement routines and cup configurations were otherwise the same as for H-cone analyses.

Solution analysis measurement of oxide formation rates was conducted using the X-cone with dynamic measurement routines. In all solution routines integration times of 4.194 seconds were used with a magnet settling time of 3.0 seconds. For Hf-oxide determination the above Yb–Lu–Hf masses were measured followed by measurement of ^{189}YbO, ^{191}LuO, ^{192}HfO, ^{193}HfO, ^{194}HfO, ^{195}HfO and ^{196}HfO. This cycle was repeated 20 times per analysis. For REE-oxide determination the same Yb–Lu–Hf masses were measured first, followed by ^{160}Gd, ^{162}Dy, ^{164}Dy, ^{165}Ho, ^{166}Er, ^{167}Er, ^{168}Er, ^{169}Tm and ^{171}Yb, repeated for 20 cycles (Table 2). All dynamic routines use the Yb–Lu–Hf cup configuration as their basis with modified zoom optics settings used to correctly align peaks for the Gd–Dy–Er–Yb and Hf-oxide peak configurations.

Laser ablation analyses used the same cup configurations and measured masses as solution analyses. For laser ablation measurement of Yb–Lu–Hf isotope data an off-peak baseline measurement is followed by 500 integrations of 0.262 seconds on the Yb, Lu and Hf masses outlined above. This incorporates 30 seconds of an on-peak gas background and up to 100 seconds of analysis. For REE-oxide-Hf analyses of zircon a dynamic measurement routine was used that incorporates 15 blocks, each consisting of 10 integrations on Yb–Lu–Hf masses, followed by one integration on Hf-oxide masses and one integration on Gd–Dy–Er–Yb masses. All integrations use a 0.524 second dwell time with a 1.5 second magnet settling time employed between mass jumps (similar to that used by Kemp *et al.*[6]). A 50 μm laser spot size, 5 Hz pulse rate and energy of 7–10 J cm^{-2} was used for all laser ablation analyses. Ablation was conducted in a He atmosphere with He flow rates of 0.8–1.0 l min^{-1} for analyses when tuning focused purely on obtaining maximum signal. 'Sample' Ar was added downstream of the ablation cell at flow rates of 0.9–1.1 l min^{-1} ('Auxiliary' Ar gas flow = 0.7 l min^{-1}). The current procedures for the facility include the addition of N_2 to the Ar sample gas flow (upstream of mixing with He) with lower He flow rates of 0.6–0.8 l min^{-1}. X-cone was used for all laser ablation analyses.

Data reduction of Yb–Hf solution and some zircon data was undertaken using a macro-driven Hf isotope data reduction Excel™ (Microsoft, 2007) spreadsheet, *HfTRAX*, coded by and available upon request from the corresponding author. Mass bias is corrected using an exponential mass bias relationship. The spreadsheet provides the option to calculate both Yb (Method 1) and Hf (Method 2) mass bias-based Yb interference corrections. Unless otherwise noted, Yb mass bias was directly measured and used to correct Yb and Lu interferences on Hf. The Yb isotopic composition of Segal *et al.*[8] is used. Lu is assumed to have the same mass bias as Yb and a Lu isotopic composition of ^{176}Lu/^{175}Lu = 0.02655.[13] All data are corrected with the Hf mass bias factor derived using ^{179}Hf/^{177}Hf = 0.7325.[14] An outlier rejection threshold of 3σ was used. All analytical uncertainties are reported at 2SE. Data reduction of REE–Hf data and zircon data was undertaken using a second spreadsheet that enables correction of both isobaric and molecular interferences on Hf isotope data. Details on the correction routine are provided in Appendix 1.†

During the period of this study two Hf isotope standards were analysed on a routine basis: JMC475 Hf isotope standard and an additional in-house isotope standard produced from an AMES Hf metal. A number of cross-calibration runs of the AMES Hf isotope standard with the JMC475 standard were done to establish a known value. Two additional cross-calibration runs were undertaken at Macquarie University (methods following[2,15]). In this study, analysis of JMC475 provides an average ^{176}Hf/^{177}Hf value of 0.282156 ± 6.1 × 10^{-6} (n = 22, 1SD; not including those analyses in Appendix 2†). Analyses of AMES yield an average ^{176}Hf/^{177}Hf value of 0.282357 ± 8.4 × 10^{-6} (n = 22, 1SD). The average ^{178}Hf/^{177}Hf values of analyses of these materials are 1.46726 ± 2.7 × 10^{-5} and 1.46726 ± 1.3 × 10^{-5}, respectively (n = 22, 1SD). The average ^{176}Hf/^{177}Hf value of the AMES metal when corrected on a session-by-session basis to a JMC475 ^{176}Hf/^{177}Hf value of 0.282160 is 0.282360 ± 4.9 × 10^{-6} (n = 22, 1SD (not propagating uncertainty from normalisation to JMC475)). The JMC475 corrected ^{176}Hf/^{177}Hf value of analyses of the AMES metal conducted at GEMOC is 0.282357 ± 1.4 × 10^{-6} (n = 8, 1SD (not propagating uncertainty from normalisation to JMC475)). A combined average of all analyses indicates a ^{176}Hf/^{177}Hf value of 0.282360 ± 4.5 × 10^{-6} (1SD) is the

Table 2 Cup configuration for dynamic analysis routines used on UofA Neptune

Cup	L4	L3	L2	L1	Axial	H1	H2	H3	H4
Configuration[a]									
Yb–Lu–Hf	^{171}Yb	^{173}Yb	^{175}Lu	^{176}Hf	^{177}Hf	^{178}Hf	^{179}Hf	^{180}Hf	—
REE	^{160}Gd	^{162}Dy	^{164}Dy	^{165}Ho	^{166}Er	^{167}Er	^{168}Er	^{169}Tm	^{171}Yb
Oxide	^{187}YbO	^{189}YbO	^{191}LuO	^{192}HfO	^{193}HfO	^{194}HfO	^{195}HfO	^{196}HfO	—

[a] Only the primary mass of interest is given for each cup position.

appropriate value for batch Hf-A4-5896 of the AMES Hf metal. This value differs from that obtained by Blichert-Toft *et al.*[16] for a sample of AMES Hf metal ($^{176}Hf/^{177}Hf = 0.282160$). However, the difference is sufficiently large that it cannot be attributed to analytical error and instead must represent a variation in the isotopic composition of Hf metal supplied by AMES over the period between production of the two samples. In order to differentiate between differing AMES metals we will refer to the standard employed here as AMES-5896.

Experimental results

Isobaric interference investigations

Analytical results for Yb isobaric interference corrections from solution and laser ablation MC-ICP-MS analyses are provided in Appendices 2 and 3,† respectively.

Results from Yb–Hf solution analyses are provided in Fig. 1. Fig. 1a displays the interference and mass bias corrected $^{176}Hf/^{177}Hf$ results for pure and Yb-spiked JMC475 Hf solutions analysed using the 'H-cone' skimmer cone. The data do not show a consistent increase or decrease in $^{176}Hf/^{177}Hf$ with increasing $^{176}Yb/^{177}Hf$. A robust regression constructed through the data yields a positive slope of 9×10^{-6} $+1.5 \times 10^{-5}/-1.2 \times 10^{-5}$ that results in a calculated change of 5×10^{-6} across the measured $^{176}Yb/^{177}Hf$ range (regression intercept $= 0.282153 \pm 6 \times 10^{-6}$; Isoplot 4.11 (ref. 17)). The significantly higher uncertainty on the regression slope, and also on the measured ratios, highlights that this trend is not statistically significant. Fig. 1b displays the mass bias corrected $^{173}Yb/^{177}Hf$ and $^{176}(Yb + Hf)/^{177}Hf$. A robust regression calculated through these data provides a slope of $0.793930 \pm 1.7 \times 10^{-5}$ (0.793997 ± 0.000095 using 'normal' York-fit regression). This slope correlates to the empirically derived $^{176}Yb/^{173}Yb$ ratio as discussed for $^{176}Yb/^{172}Yb$ by Griffin *et al.*[15] When data from individual analysis session are used the calculated slopes range from 0.793920 to 0.794027. For the purposes of laser ablation analyses the 'X-cone' skimmer cone is used and hence it is necessary to repeat these solution analyses using the X-cone. Fig. 1c displays the interference and mass bias corrected $^{176}Hf/^{177}Hf$ results for pure and Yb-spiked JMC475 Hf solutions (using X-cone). A robust regression through these data yields an intercept of $0.282150 \pm 3 \times 10^{-6}$ and a positive slope of 2.3×10^{-5} $+1.2 \times 10^{-5}/-1.6 \times 10^{-5}$. Mass bias corrected $^{173}Yb/^{177}Hf$ and $^{176}(Yb + Hf)/^{177}Hf$ data for the X-cone dataset yield a robust regression with a slope of $0.793777 \pm 2.3 \times 10^{-5}$ (0.793750 ± 0.00061 using 'normal' York-fit regression).

Results from the laser ablation Yb–Hf glass bead analyses are provided in Fig. 2, which displays interference and mass bias corrected $^{176}Hf/^{177}Hf$ data with ^{176}Yb interference correction using Methods 1 (Yb fractionation factor corrected) and 2 (Hf fractionation factor corrected with empirically derived $^{176}Yb/^{173}Yb$) as described above. Natural ratios of $^{171}Yb/^{173}Yb = 0.884821$ and $^{176}Yb/^{173}Yb = 0.793813$ (ref. 8) are used for Method 1. With increasing $^{176}Yb/^{177}Hf$ ratios the interference corrected $^{176}Hf/^{177}Hf$ ratios trend downwards, however all but three analyses are within uncertainty of the 'true' $^{176}Hf/^{177}Hf$ ratio. Data corrected using the Hf fractionation correction method (Method 2) and the H-cone $^{176}Yb/^{173}Yb$ ratio of

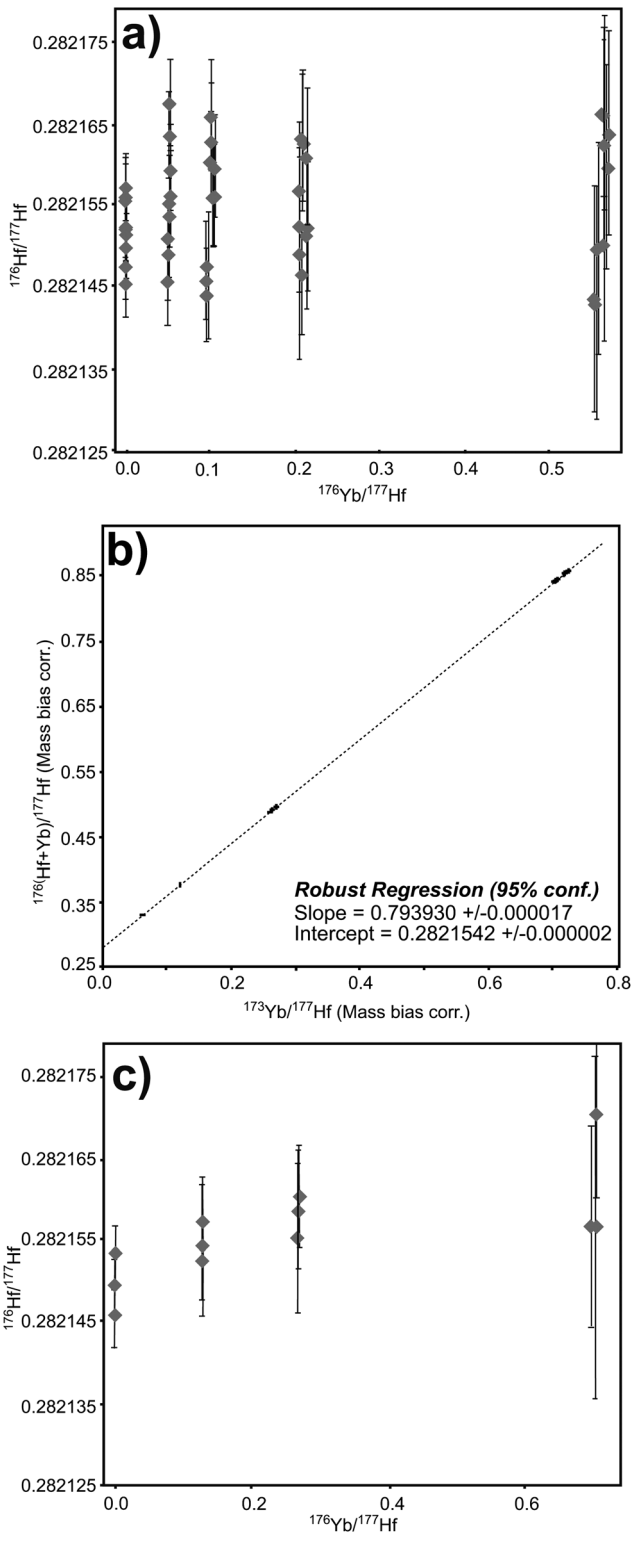

Fig. 1 (a) Interference corrected $^{176}Hf/^{177}Hf$ data for Yb-doped JMC475 Hf standard solutions showing accurate $^{176}Hf/^{177}Hf$ ratios for all solutions. Data are corrected using an interference correction (Method 1) in which ^{176}Yb is calculated from a Yb fractionation factor derived from measured $^{171}Yb/^{173}Yb$ ratios. (b) Mass bias corrected $^{173}Yb/^{177}Hf$ *versus* mass bias corrected $^{176}(Hf + Yb)/^{177}Hf$ for Yb-doped JMC475 Hf standard solution analyses. Linear regression is discussed within the text. (c) Interference corrected $^{176}Hf/^{177}Hf$ data for Yb-doped JMC475 Hf standard solutions using the X-cone and Method 1 ^{176}Yb interference correction.

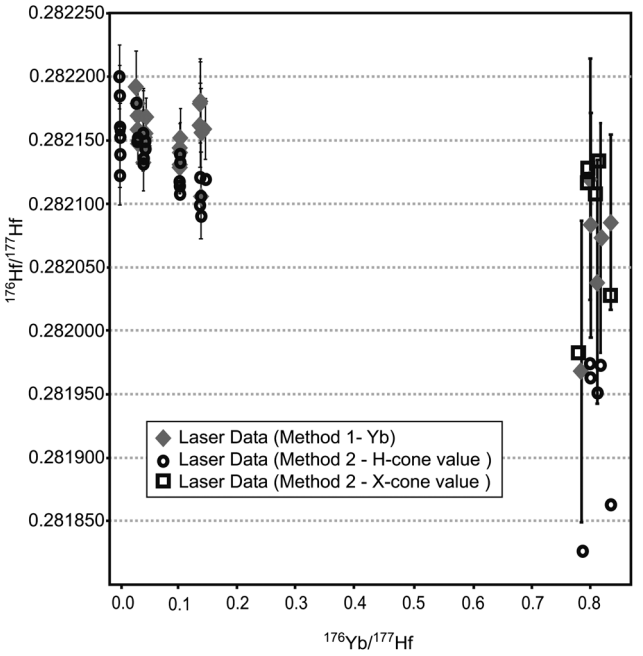

Fig. 2 Interference and mass bias corrected $^{176}Hf/^{177}Hf$ data for Yb-doped JMC475 Hf glass beads. Data are corrected using interference correction Method 1 with values of Segal *et al.*[8] and X-Cone Method 2 using the empirically derived ratio from solution analyses using the H-cone ($^{176}Yb/^{173}Yb = 0.793930$) and X-cone ($^{176}Yb/^{173}Yb = 0.793777$). Method 2 corrected values for low $^{176}Yb/^{177}Hf$ analyses are not included for clarity of diagram but fall within the range of Method 1 values.

0.793930 are consistently lower than the equivalent Yb–Yb fractionation corrected method. This difference between the two methods increases at higher $^{176}Yb/^{177}Hf$ ratios. Conversely, the data corrected using Method 2 and the X-cone $^{176}Yb/^{173}Yb$ ratio of 0.793777 are distributed above and below the Method 1 data and are statistically indistinguishable. A robust regression calculated through the mass bias corrected $^{173}Yb/^{177}Hf$ and $^{176}(Yb + Hf)/^{177}Hf$ data obtained from the Yb–Hf glass beads provides a slope of $0.793689 \pm 8.8 \times 10^{-5}$ (0.793666 ± 0.000083 using 'normal' York-fit regression). This value is statistically different to the equivalent value obtained from solution analysis using the H-cone but within uncertainty of the value derived using the X-cone analyses. This suggests differences in mass bias relationships are more dependent upon changes in the interface region (*e.g.* skimmer cone geometry) as opposed to sample introduction method of solution *versus* laser ablation.

Molecular interference investigations

Results for molecular interference corrections from solution and laser ablation MC-ICP-MS analyses are provided in Appendices 4 and 5,† respectively.

Measurement of single element solutions on the University of Adelaide (UofA) Neptune yielded weighted averages of relative oxide formation rates (normalised to Hf oxide formation rate) of 5.06 for Gd, 0.29 for Dy. Results from analysis of Gd–Tb–Dy doped JMC475 Hf solutions are provided in Fig. 3a. The results corrected from these analyses using the normal isobaric interference and mass bias correction routine demonstrate a positive correlation between REE concentration and isobaric interference and mass bias corrected $^{176}Hf/^{177}Hf$. The same data corrected for molecular (REE oxide) and isobaric interferences and mass bias all plot within uncertainty (2SE) of the weighted average of the pure JMC475 Hf standard analyses (Fig. 3a, details of correction procedure in Appendix 1†). Hf oxide formation rates for this set of analyses are in the range 1.64–1.68% (Appendix 4†).

Analysis of single element or REE and Hf doped glass beads was undertaken using laser ablation on the UofA Neptune. Over the course of one year, the relative GdO to HfO formation rate varied between 3.08 and 11.4 with the highest relative oxide formation rate being recorded in the analytical session used for the analysis of the natural zircon samples reported in this study (Fig. 3b).

Results from analyses of the Gd and Hf doped glass beads are provided in Fig. 3c. These data show a positive correlation between REE concentration and $^{176}Hf/^{177}Hf$ when uncorrected for molecular interferences. When these data are corrected for molecular interferences assuming the relative Hf and Gd oxide formation rate derived from solution analyses, a positive correlation with REE concentration remains. As no Yb or Lu is present in the glass beads it is also possible to directly calculate the oxide formation rate based upon the deviation of the data from the correct $^{176}Hf/^{177}Hf$ value. This can be done in a number of ways. One method is to calculate iteratively the relative GdO formation rate (relative to the measured HfO/Hf) that is required to correct each individual analysis back to the 'true' value ($^{176}Hf/^{177}Hf = 0.282160$) and then average these relative formation rates. This approach yields an average relative GdO formation rate of 11.28 ($1\sigma = 0.749$, $n = 20$). This approach is limited by the assumption that the only reason a non-true value would be obtained for the analysis is due to GdO interferences. Hence it creates a circular argument for internally correcting oxide formation rates for this dataset. A robust regression of all the data using the mass bias corrected $^{176}(Hf + Gd)/^{177}Hf$ and $^{160}Gd/^{177}Hf$ (assuming Gd mass bias is the same as Hf mass bias) yields an intercept value (*i.e.* no GdO interference) of $0.282156 \pm 4 \times 10^{-6}$. This results highlights the general applicability of the 0.282160 value but also demonstrates that some variation from 'true' does occur. An alternative method is to calculate a regression between the $^{160}Gd/^{177}Hf$ and $^{176}(Hf + Gd)/^{177}Hf$ data (not mass bias corrected) with the resultant slope equivalent to the GdO formation rate. This approach is limited by uncertainty in determining the appropriate HfO formation rate to use for a given analytical session. We have chosen to use the mean Hf oxide formation rate from analyses of the highest Gd content bead because, due to its outlying composition, it will provide the greatest individual control on the regression slope and hence calculated GdO formation rate. The result is a relative GdO formation rate of 11.40. The two calculated relative GdO formation rates are within uncertainty of each other but result in slight differences in corrected data, such that data corrected using 11.28 relative GdO formation rate yields a weighted mean of $^{176}Hf/^{177}Hf = 0.282154 \pm 11 \times 10^{-6}$ whilst data corrected using a value of 11.40 yields a weighted mean of $^{176}Hf/^{177}Hf = 0.282146 \pm 12 \times 10^{-6}$.

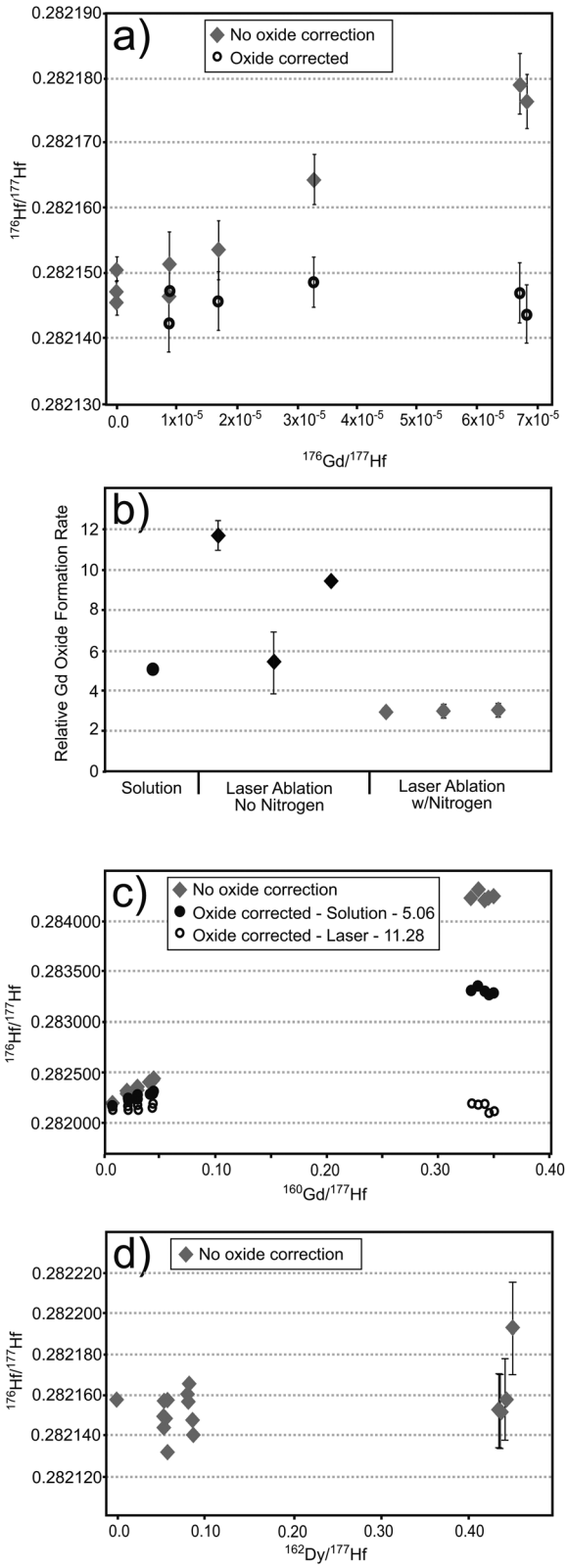

Fig. 3 (a) Mass bias corrected $^{176}Hf/^{177}Hf$ data for Gd–Dy–Tb doped JMC475 Hf solutions and mass bias and oxide interference corrected data for the same analyses. (b) Variation in relative Gd oxide formation rates compared to Hf oxide formation rates. Data were collected over a 12 month period and each data point represents 3 to 5 measurements of Gd and Hf solutions or glass beads. (c) Mass bias and non-oxide corrected and oxide corrected data for analysis of Gd and Hf doped glass beads. Oxide corrections undertaken using relative oxide formation rate obtained from solution analyses and from laser ablation analyses. (d) Mass bias corrected data for analysis of Dy and Hf doped glass beads demonstrating a lack of identifiable DyO interference.

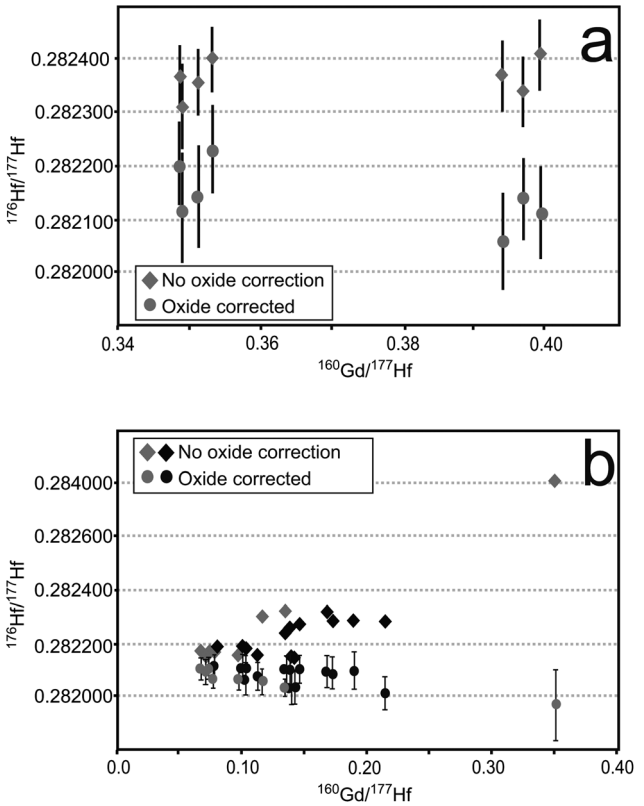

Fig. 4 (a) LA-MC-ICP-MS data for 'zircon' REE composition glass bead with and without oxide corrections. (b) LA-MC-ICP-MS data for natural zircon sample F834. Data collected in 2 sessions as represented by the grey and black symbol colour. All data are corrected for mass bias and isobaric interferences with oxide interferences undertaken using a relative GdO formation rate of 11.28.

Results from analyses of Dy and Hf doped glass beads are displayed in Fig. 3d. As suggested by low relative oxide formation rates of Dy and theoretical calculations (see Discussion), $^{176}Hf/^{177}Hf$ values show no discernible correlation with increasing Dy/Hf ratios.

Natural zircon and zircon REE-composition glass beads

Data for the zircon REE-composition glass bead are presented in Fig. 4a and Appendix 5.† These glass beads yield $^{176}Yb/^{177}Hf$ of 0.35–0.40, $^{160}Gd/^{177}Hf$ of 0.019–0.022 and $^{162}Dy/^{177}Hf$ of 0.082–0.09. Data corrected only for isobaric interferences and mass bias yield a weighted average $^{176}Hf/^{177}Hf$ of 0.282263 ± 0.000035 (n = 7, 2σ). Data corrected using the oxide correction routine outlined in Appendix 1† yield a weighted average $^{176}Hf/^{177}Hf$ of 0.282146 ± 0.000055 (n = 7, 95% conf.) using the relative GdO formation rate of 11.28 or 0.282144 ± 0.000056 (n = 7, 95% conf.) using the relative GdO formation rate of 11.40.

LA-MC-ICP-MS data for the natural zircon population from sample F834-147.5 are presented in Fig. 4b and Table 3. This

Table 3 LA-MC-ICP-MS Lu–Hf isotope data for natural zircon sample F834-147.5

								No oxide corr.						
Analysis no.	Total Hf beam (V)	$^{176}Hf/^{177}Hf$	2SE	Hf Fract. factor	2SE	$^{178}Hf/^{177}Hf$	2SE	$^{176}Yb/^{177}Hf$	$^{176}Lu/^{177}Hf$	$^{160}Gd/^{177}Hf$	$^{162}Dy/^{177}Hf$	$^{176}Hf/^{177}Hf$	2SE	$^{196}HfO/^{180}Hf$ (%)
Session 1														
F834_01	7.29	0.282068	3.6×10^{-5}	0.8826	4.9×10^{-3}	1.46731	8.5×10^{-5}	0.0656	0.0010	0.0097	0.0510	0.282168	4.2×10^{-5}	0.124
F834_02	6.63	0.281971	1.3×10^{-4}	0.8536	7.2×10^{-3}	1.46740	1.3×10^{-4}	0.3054	0.0045	0.1190	0.3835	0.282813	1.5×10^{-4}	0.120
F834_03	6.78	0.282105	3.8×10^{-5}	0.8636	4.3×10^{-3}	1.46734	8.1×10^{-5}	0.0627	0.0011	0.0065	0.0293	0.282173	4.2×10^{-5}	0.117
F834_04	5.88	0.282106	4.2×10^{-5}	0.8639	5.4×10^{-3}	1.46729	9.0×10^{-5}	0.0576	0.0010	0.0080	0.0322	0.282172	4.2×10^{-5}	0.119
F834_05	6.45	0.282057	5.0×10^{-5}	0.8413	4.5×10^{-3}	1.46733	8.5×10^{-5}	0.1000	0.0016	0.0335	0.1070	0.282304	4.7×10^{-5}	0.116
F834_06	6.78	0.282033	3.3×10^{-5}	0.8415	4.9×10^{-3}	1.46729	6.1×10^{-5}	0.1162	0.0018	0.0413	0.1372	0.282325	4.1×10^{-5}	0.112
F834_07	6.26	0.282092	4.6×10^{-5}	0.8269	5.8×10^{-3}	1.46736	9.9×10^{-5}	0.0605	0.0010	0.0067	0.0298	0.282157	4.6×10^{-5}	0.113
F834_08	6.38	0.282066	4.1×10^{-5}	0.8239	4.8×10^{-3}	1.46728	7.3×10^{-5}	0.0835	0.0014	0.0130	0.0477	0.282157	4.1×10^{-5}	0.105
Session 2														
F834_02b	7.39	0.282106	5.2×10^{-5}	1.0643	6.7×10^{-3}	1.46725	1.5×10^{-4}	0.0861	0.0013	0.0183	0.0788	0.282191	5.5×10^{-5}	0.062
F834_09	6.77	0.282115	4.9×10^{-5}	1.0532	6.3×10^{-3}	1.46743	1.1×10^{-4}	0.0667	0.0012	0.0088	0.0376	0.282178	4.3×10^{-5}	0.061
F834_10	5.73	0.282102	5.1×10^{-5}	1.0501	7.2×10^{-3}	1.46721	1.4×10^{-4}	0.1171	0.0020	0.0220	0.0792	0.282236	5.1×10^{-5}	0.059
F834_11	5.40	0.282077	5.2×10^{-5}	1.0553	7.4×10^{-3}	1.46727	1.5×10^{-4}	0.0968	0.0018	0.0148	0.0574	0.282154	4.9×10^{-5}	0.061
F834_12	5.94	0.282088	6.2×10^{-5}	1.0859	1.0×10^{-2}	1.46730	2.0×10^{-4}	0.1492	0.0025	0.0407	0.1415	0.282284	6.1×10^{-5}	0.055
F834_13	6.22	0.282013	6.2×10^{-5}	1.0922	5.8×10^{-3}	1.46729	1.3×10^{-4}	0.1860	0.0029	0.0756	0.1977	0.282275	6.4×10^{-5}	0.053
F834_14	5.61	0.282105	4.7×10^{-5}	1.0948	7.9×10^{-3}	1.46738	1.4×10^{-4}	0.0884	0.0015	0.0159	0.0447	0.282174	4.6×10^{-5}	0.051
F834_15	5.78	0.282103	5.2×10^{-5}	1.1134	6.7×10^{-3}	1.46734	1.2×10^{-4}	0.1264	0.0020	0.0461	0.1366	0.282268	5.3×10^{-5}	0.053
F834_16	5.86	0.282095	5.9×10^{-5}	1.0932	5.8×10^{-3}	1.46731	1.3×10^{-4}	0.1454	0.0024	0.0535	0.2108	0.282313	5.7×10^{-5}	0.057
F834_17	5.50	0.282098	7.1×10^{-5}	1.0857	8.2×10^{-3}	1.46731	2.1×10^{-4}	0.1643	0.0027	0.0513	0.1605	0.282288	7.3×10^{-5}	0.054
F834_18	6.72	0.282101	6.6×10^{-5}	1.0915	7.3×10^{-3}	1.46720	1.9×10^{-4}	0.1199	0.0018	0.0368	0.1123	0.282258	6.3×10^{-5}	0.052
F834_19	5.93	0.282034	6.3×10^{-5}	1.0878	6.4×10^{-3}	1.46725	1.5×10^{-4}	0.1229	0.0018	0.0316	0.0988	0.282146	6.2×10^{-5}	0.052
F834_20	5.65	0.282065	5.9×10^{-5}	1.0967	8.0×10^{-3}	1.46737	1.6×10^{-4}	0.0886	0.0014	0.0347	0.0932	0.282175	5.9×10^{-5}	0.050
F834_21	5.90	0.282034	6.5×10^{-5}	1.0733	8.4×10^{-3}	1.46724	1.8×10^{-4}	0.1211	0.0020	0.0308	0.1013	0.282149	6.5×10^{-5}	0.048

zircon population was separated from a 0.5 m thick felsic volcanic tuff that occurs within laminated carbonates in the middle Fifteenmile Group in the western Ogilvie Mountains, Yukon, Canada. A subset ($n = 4$) of the original zircon population dated by chemical abrasion ID-TIMS yielded a weighted mean $^{206}Pb/^{238}U$ age of 811.51 ± 0.25 Ma (MSWD = 0.07 (ref. 18)). Lu–Hf data uncorrected for oxide interferences shows a positive correlation with increasing Yb and Gd content. Data corrected using the relative GdO formation rate derived from solution analysis also show a positive correlation whilst data corrected using the laser ablation derived value of 11.28 all plot within uncertainty of the each other and do not show a trend with increasing REEs.

Discussion

The experiments and theoretical calculations of this study are designed to test the robustness of the isobaric interference corrections used and also demonstrate the potential impacts of molecular interferences on *in situ* Lu–Hf isotope measurements.

Theoretical considerations of molecular interferences

The potential implications of molecular interferences on isotope ratio accuracy can be estimated by theoretical simulation. These calculations are relatively simple but a number of different factors need to be considered in order for them to accurately represent the variability and potential extent of molecular (REE-oxide) interferences in actual analyses. Table 1 provides a summary of the isotope proportions of Yb, Lu and Hf and the interfering rare earth element (REE) oxides (assuming mass of O to be 16 amu). This highlights the complexity of the measurements and correction methods when REE oxides are taken into account as Yb, Lu and Hf all have potential REE oxide interferences of varying magnitudes. In order to model and correct for molecular interferences it is necessary to take into account the oxide formation rate for individual elements within the analysis and the relative concentrations of all of the elements of interest.

During LA-MC-ICP-MS analyses it is not possible to directly measure the REE-oxide formation rates. However, Hf oxide formation rates can be readily measured as there are no elements of the same mass as the Hf oxides (*i.e.* Ir and Pt) within the minerals of interest. A relationship between Hf and REE oxide formation rates is then required to determine the REE oxide formation rates during any given analysis. Oxide formation for individual rare earth elements within ICP-MS instruments has been demonstrated to be correlated to the metal oxide (MO^+) bond energy.[19,20] Due to the importance of using appropriate relative oxide formation rates in analytical interference corrections we have measured the relative oxide formation rates of Hf, Dy and Gd using a variety of instruments and methods. We apply relative (to HfO) oxide formation rates for Gd and Dy of 5.06 and 0.29 (as determined by solution analyses on the UofA Neptune). As will be discussed later these relative rates differ from those predicted by MO^+ bond energies.

In order to fully represent the compositional range of natural zircon it is necessary to consider both the relative concentrations of total REEs to Hf in addition to the relative concentrations of Gd and Dy to Yb, Lu and Hf. These relative concentrations are easily apparent in the steepness of chondrite-normalised 'spider' plots. Examples of REE patterns found in natural zircons are plotted in Fig. 5a. The dataset of Belousova *et al.*[21] gives a natural zircon composition range of $^{176}Lu/^{177}Hf = 4 \times 10^{-6}$ to 0.005 and $^{176}Yb/^{177}Hf = 0.0002$ to 0.192 ($n = 10\,488$). The natural zircon grains analysed in this study include $^{176}Yb/^{177}Hf$ values up to 0.31 with 12 of the 22 analyses from the sample yielding compositions above 0.1. In the dataset of Belousova *et al.*[21] zircon yields Gd : Lu ratios in the range of 0.0294 to 3.632 and Dy to Lu ratios of 0.7167 to 6.737 (Fig. 5b). Fig. 5b demonstrates the range in REE patterns of four commonly used zircon standards, highlighting the relatively low REE/Hf compositions of the standards but the large variation in Gd/Lu and Dy/Lu values. In an attempt to make the theoretical models as realistic as possible we use a starting REE pattern taken from an analysis of the Mud Tank zircon standard. This also makes use of the measured mass bias relationships of the different elements and enhances the expected accuracy of the calculations. The analytical data provide starting isobaric interference ratios of $^{176}Lu/^{177}Hf = 0.00002$ and $^{176}Yb/^{177}Hf = 0.0011$. These ratios equate to elemental ratios of Lu/Hf = 0.00013 and Yb/Hf = 0.0017. Dy and

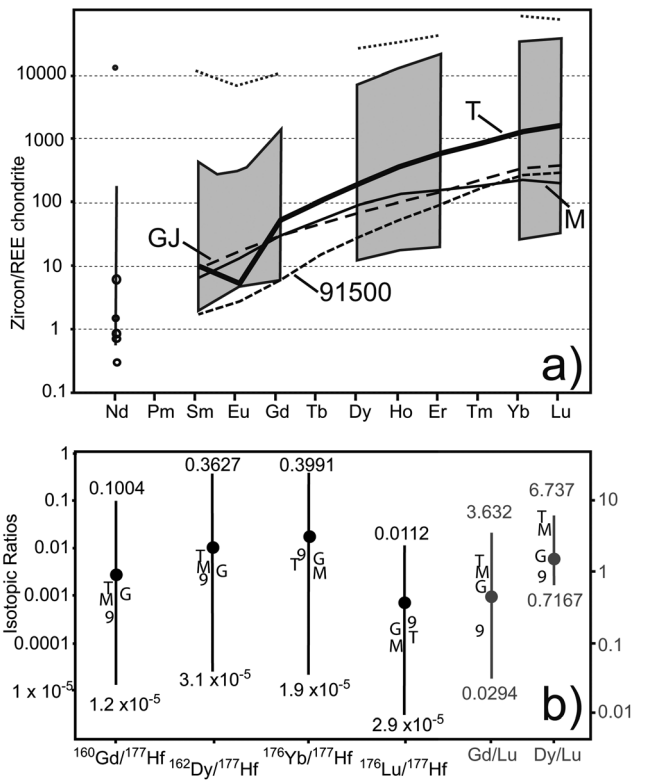

Fig. 5 (a) Example REE 'spiderplots' for a range of natural zircon standards and natural zircon grains[21] (normalised to chondrite[23]). (b) Ranges of isotopic and elemental ratios in natural zircons from Belousova *et al.*[21] and selected common zircon standards. Symbols are: 9–91 500, T – Temora, M – Mud Tank, G – GJ-1.

Gd were set to values of Dy/Hf = 0.0005 and Gd/Hf = 0.00015 or Dy/Lu = 3.754 and Gd/Lu = 1.120 based upon the Mud Tank zircon analysis. The REE concentrations relative to Hf were tested at various levels up to 200 times that of the starting concentrations. This yields maximum ratios of Lu/Hf = 0.0264 and Yb/Hf = 0.332. Lu and Yb concentrations of 100 times the starting composition (Lu/Hf = 0.0132, Yb/Hf = 0.166) were chosen to test the impact of differing REE patterns by varying the levels of Dy and Gd. At the set Lu and Yb levels, the ranges used were Gd/Lu = 0.280–2.240 and Dy/Lu = 0.9384–7.507. This range in Gd/Lu values encompasses the composition of the zircon standards provided in Fig. 5b and the majority of zircons in Belousova *et al.*[21]

Results of the theoretical calculations are presented in Fig. 6. For each of the compositions described above, the interferences and resultant effects on Hf and Yb mass bias factors and Hf isotopic ratios were calculated using GdO formation rates of 0 to 20%. In Fig. 6, only oxide formation rates up to 2% GdO are presented. For the relative oxide formation values obtained *via* solution analysis in this study, a GdO formation rate of 0.1% equates to HfO formation rate of 0.0198% and similarly 2% GdO equates to 0.395% HfO. Mass bias is corrected using an exponential mass bias law and the $^{171}Yb/^{173}Yb$ ratio for Yb and Lu and the $^{179}Hf/^{177}Hf$ ratio for Hf.

Fig. 6a displays the isobaric interference and mass-bias corrected $^{176}Hf/^{177}Hf$ ratios for varying levels of REE concentration (using the Mud Tank REE pattern) and oxide formation. It is evident from these data that oxide interferences (even for modest oxide formation rates) affect the calculated $^{176}Hf/^{177}Hf$ ratios. For a REE pattern such as found in Mud Tank, this results in deviations greater than typical 2SE of 2×10^{-5} at Gd oxide formation rates of 0.5% and $^{176}Yb/^{177}Hf = 0.102$ (Yb/Hf = 0.149, Lu/Hf = 0.012, Gd/Hf = 0.0133). For the given REE distribution, low oxide formation rates (*i.e.* <0.2%) result in a systematic error in the measurement but on a single analysis this error is likely to be within uncertainty of the true value. The Hf mass bias factor (Fig. 6b) is increased with oxide interferences resulting in a higher calculated $^{176}Hf/^{177}Hf$ ratio. However, for oxide formation rates of 0.5% and $^{176}Yb/^{177}Hf =$ 0.102 the $^{176}Hf/^{177}Hf$ ratio is increased by less than 2×10^{-6} due to Hf mass bias factor alone. ^{176}Yb is over-corrected as a result of the increased apparent ^{173}Yb signal due to the ^{173}GdO interference. For GdO = 0.5% and the above listed composition, the $^{176}Hf/^{177}Hf$ is decreased by 4×10^{-5} due to the over-correction from the erroneous ^{173}Yb value. This over-correction is lessened (it would otherwise be 4.5×10^{-5}) by the decrease in Yb mass bias factor due to the GdO interferences on ^{171}Yb and ^{173}Yb. However, the Yb over-correction is outweighed by the direct ^{176}GdO interference on ^{176}Hf which equates to an increase in $^{176}Hf/^{177}Hf$ by 8×10^{-5} for the same conditions. In combination these interferences result in the observed increase in $^{176}Hf/^{177}Hf$ of 4×10^{-5}.

Fig. 6c displays the variation evident in calculated $^{176}Hf/^{177}Hf$ ratios for a constant Yb and Lu content but varying REE composition. For a Gd value twice that present in a 'normal' Mud Tank REE distribution (marked in Fig. 6c) the $^{176}Hf/^{177}Hf$ value is effectively identical to that produced by a doubled normal REE distribution composition. The differences in Yb mass bias factor and proportion of ^{173}X signal that is ^{173}GdO effectively cancel each other out at the levels of precision used for the $^{176}Hf/^{177}Hf$ ratio (*i.e.* 10^{-6}). This highlights the sensitivity of oxide interferences only to the actual interfering elements (namely Gd), independent of Yb and Lu, and therefore

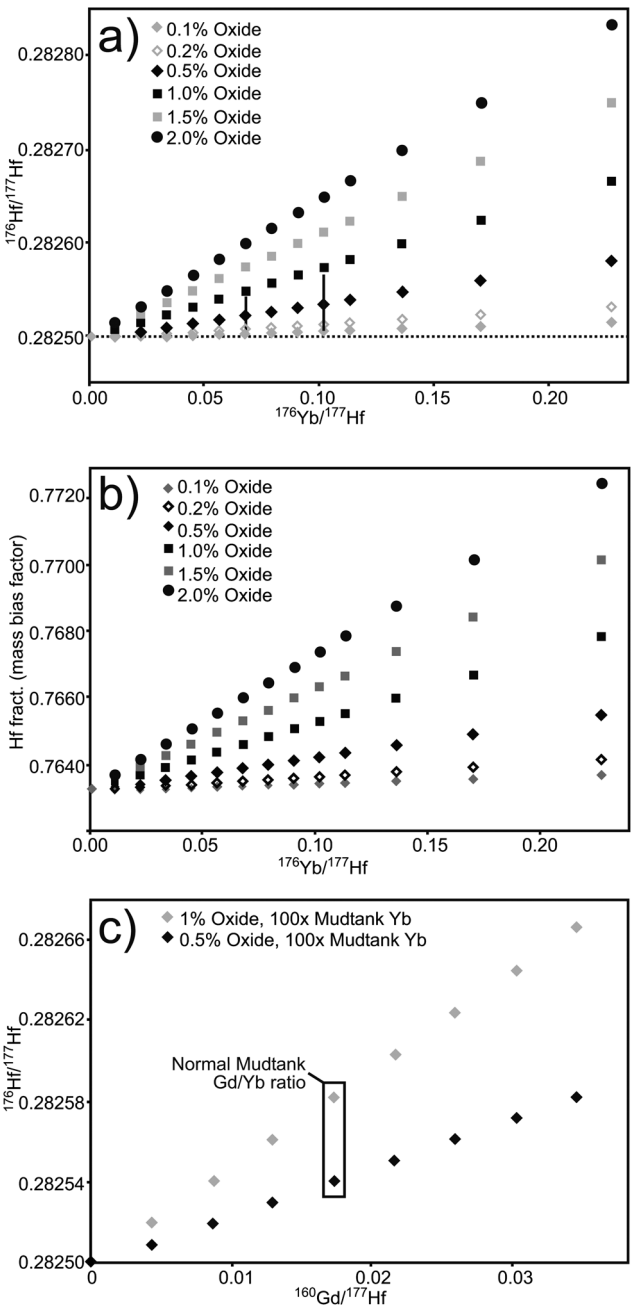

Fig. 6 (a) Theoretical isobaric interference and mass bias corrected $^{176}Hf/^{177}Hf$ values for increasing REE content analyses (with Mud Tank REE pattern) and varying Gd oxide formation rates. Representative uncertainty of typical 2SE is shown as error bars for two data points. (b) Predicted variation in Hf mass bias factors due to oxide formation ($^{176}Yb/^{177}Hf = 0.102$ with Mud Tank REE pattern). (c) Variation in isobaric interference and mass bias corrected $^{176}Hf/^{177}Hf$ values for varying Gd and Dy concentrations with Lu and Yb concentrations of 100 times normal Mud Tank composition.

the use of Yb/Hf or Lu/Hf ratios to ascertain if there is a correlation between $^{176}Hf/^{177}Hf$ and REE concentrations may be a false premise (for the Yb mass bias correction method).

Isobaric and molecular interferences and their correction

An often cited criticism of the *in situ* LA-MC-ICP-MS method is a lack of natural zircon standards that encompass the full compositional range of analysed natural zircon. This problem is compounded by the observation that some datasets show a positive correlation between Yb content and $^{176}Hf/^{177}Hf$ values. Fisher *et al.*[4] addressed this issue by manufacturing a series of synthetic zircon crystals doped with REEs and Hf with $^{176}Yb/^{177}Hf$ ratios as high as 0.48. They demonstrated the ability to adequately correct for isobaric interferences in the synthetic zircon. Our results further highlights the robustness of isobaric interference corrections as we have demonstrated the capability of accurately correcting for $^{176}Yb/^{177}Hf$ values up to 0.7 in solution analyses and up to 0.15 in laser ablation analyses. The robustness of the correction for solutions in which ^{176}Yb vastly exceeds ^{176}Hf is particularly encouraging and highlights the applicability of the exponential mass bias law and Yb isotope values of Segal *et al.*[8] Laser ablation analyses with $^{176}Yb/^{177}Hf$ values up to 0.8 are also largely within uncertainty of the true $^{176}Hf/^{177}Hf$ value. Two of these high Yb data points lie outside of uncertainty of the true value and all data points are lower than the true value (*i.e.* over-correction of interferences). Whilst these levels of isobaric interference are significantly higher than those found in natural zircon, and hence are not of concern during normal analysis, the results suggest that further study is required to determine the cause of variation between solution and laser ablation data. These data, even with the potential for an over-correction of Yb interferences at extreme $^{176}Yb/^{177}Hf$, demonstrate that the isobaric interference corrections for natural samples are valid and allow for assessment of the impact of molecular interferences in data collected on this instrument.

Fig. 4a and b highlight the potential for molecular interferences to result in measurable systematic errors for calculated $^{176}Hf/^{177}Hf$ ratios under the instrument running conditions used in this study. The analysis of solutions and glass beads without the presence of Yb and Lu allow us to demonstrate that these analytical errors are directly related to molecular interferences, namely GdO. As suggested by measured oxide production rates and theoretical modelling, the impact of DyO interferences is observed to be relatively small. Variation is only on the order of 1×10^{-5} to 2×10^{-5} for Dy/Hf ratios up to 0.33 which is typically within analytical uncertainty for high REE zircon. This Dy/Hf value is approximately 100 times that seen in the Mud Tank zircon and is at the upper limits of what would be considered the normal range for zircon. Additionally, as will be discussed later, the oxide formation rates during the relevant analytical session were the highest recorded in this study (*ca.* HfO/Hf = 0.0023) and as much as 3–10 times higher than oxide formation rates when the instrument is tuned to minimise oxide production. Under optimised running conditions the same DyO interferences would be within analytical uncertainty and not measurable.

As predicted by theoretical modelling, the GdO interferences are significant and readily detected. This highlights that oxide formation rates must be determined when analysing high-REE zircon. Because the instrument was tuned to maximise sensitivity for this study the interferences go beyond what is the normal oxide production rate for the facility, particularly because N_2 addition is now used (see discussion below). However, even at the highest oxide production rates used here the oxide production is still below what would be considered acceptable for many applications of quadrupole LA-ICP-MS.[19]

As molecular interferences can be shown to be a source of error in LA-MC-ICP-MS analysis it is useful to assess the ability to correct for these interferences. The primary test of the proposed dynamic measurement method and oxide interference correction routine (Appendix 1†) are the data collected on the zircon REE-Hf-composition glass bead containing JMC475 Hf and Lu, Yb, Er, Dy, Tb and Gd. Despite the presence of oxide interferences the data can be successfully corrected for oxide interferences. The correction routine shifts values from *ca.* 1×10^{-4} above the true $^{176}Hf/^{177}Hf$ value of JMC475 to within uncertainty of the true value. The suitability of the correction routine is further supported by the natural zircon data of sample F834-147.5. These data were collected in two analytical sessions (more than 2 months apart) and show a near linear correlation between $^{176}Hf/^{177}Hf$ and Yb/Hf when uncorrected for oxide interferences. This results in the high REE analyses being well outside of uncertainty of the low REE analyses. When the oxide correction routine is applied the data all results fall within uncertainty of each other. That the data is collected in analytical sessions with differing oxide formation rates also provides support for the long term applicability of the method. The oxide correction routine is limited in that it does not include a full propagation of uncertainties associated with the empirically derived relative oxide formation rates or the assumption that Gd has the same mass bias as Yb. However, the correction of the glass bead and natural zircon data to values within uncertainty does suggest that the uncertainties are within those generated by the large ^{176}Yb interference correction in these data. Further testing on synthetic and natural datasets is required to better constrain the within analysis uncertainties and long term reproducibility of the correction routine in order to provide a basis for full uncertainty propagation.

Relative oxide formation rates during LA-MC-ICP-MS analysis

Little information is available concerning oxide formation during Lu–Hf LA-MC-ICP-MS analysis, and few papers provide details of oxide formation rates (*e.g.* ref. 2, 3 and 22). Hence, it is difficult for us to compare our results with those obtained on other instruments. At the same time this highlights the lack of understanding of the effects of molecular interferences on any given analysis of high REE zircon. In most instances, oxide formation is not an issue because REE concentrations within most zircons are too low to generate analytically significant oxide interferences. However, in high-REE zircon, oxide production becomes important and oxide formation rates

should be reported in order to provide an additional measure of the validity of the data.

When tuned solely for maximum sensitivity without addition of N_2, HfO formation rates on the UofA/CSIRO Neptune reached as high as 0.27%, but typical HfO formation rates under this tuning regime fall in the range of 0.12–0.16%. When tuned to optimise both sensitivity and oxide formation the HfO formation rates are typically in the range 0.13–0.02%. When N_2 addition is used (such as per ref. 10), the HfO formation rates are reduced to 0.06–0.01%. Importantly there is also a significant change observed in the relative oxide formation rates (Fig. 5b) and the variation in relative oxide formation rates between sessions. Relative GdO to HfO formation rates drop to ~3 and are more consistent than relative oxide formation rates without N_2 addition. In order to verify the influence of N_2 on relative oxide formation rates, we analysed Gd and Hf glass beads within a single one hour period both with and without N_2 addition. Analyses with N_2 addition yield a mean relative GdO formation rate of 2.97 (±0.088, 1SD) whilst analyses without N_2 yield a mean relative GdO formation rate of 9.47 (±0.082, 1SD). As these two sets of analyses were conducted with near identical instrument running conditions it highlights the value of N_2 addition in reducing oxide formation rates overall, but most importantly GdO formation rates.

A number of studies have reported the correlation of REE oxide formation to the metal oxide (MO^+) bond energy.[19,20] However, corrections based on metal oxide bond energy alone cannot adequately represent the complexities of the plasma environment and variations in relative oxide formation rate caused by different sample introduction methods, gases and tuning parameters. To verify the observed oxide formation behaviour on the UofA/CSIRO instrument, oxide formation rate experiments were conducted on an Agilent 7500cs ICP-MS and a Nu Plasma MC-ICP-MS at Macquarie University. The results of these analyses are shown in Fig. 7. Collectively the data demonstrate the higher formation rate of GdO compared to HfO and the variation in relative oxide formation rates between instruments and sample introduction methods. The data do show a general positive trend between metal oxide bond energy and oxide formation rates for the REEs but the relationship is not viable for predicting oxide formation rates for the purposes of correcting interferences in isotope ratio analyses.

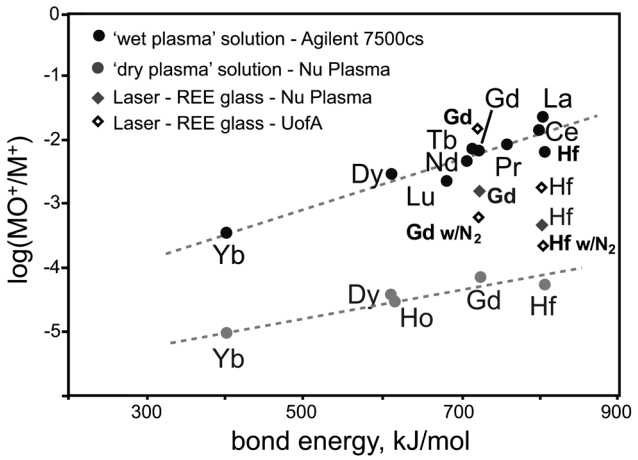

Fig. 7 Oxide formation rates for REEs and Hf as determined by solution and laser ablation analysis using UofA/CSIRO MC-ICP-MS and Macquarie University Nu Plasma MC-ICP-MS and Agilent 7500cs ICP-MS.

Conclusions

This study highlights the potential for systematic error due to molecular or oxide interferences in LA-MC-ICP-MS Lu–Hf isotope data. However, in doing so, this study also reinforces the robustness of the technique for the vast majority of natural zircon grains and provides either a criteria by which to monitor or correct for molecular interferences in high REE zircon. Similar to Fisher *et al.*,[4] we recommend the monitoring of isobaric interference, mass bias correction and oxide formation rates with daily analysis of synthetic standard materials, either zircon or glass.

Acknowledgements

This study was supported by an Institute for Minerals and Energy Resources (IMER) Strategic Research Initiative grant to Martin Hand and Justin Payne. Karin Barovich and Martin Hand are thanked for discussions regarding the analytical routine development at UofA. Francis Macdonald and Mark Schmitz kindly shared natural zircons for this study. Two anonymous reviewers are thanked for comments that helped clarify the analytical procedures and findings. The analytical data were obtained using instrumentation funded by DEST Systemic Infrastructure Grants, ARC LIEF, NCRIS, industry partners, Macquarie University, CSIRO and University of Adelaide. This is contribution 256 from TRaX, 306 from the ARC Centre of Excellence for Core to Crust Fluid Systems (http://www.ccfs.mq.edu.au) and 875 in the GEMOC Key Centre (http://www.gemoc.mq.edu.au).

References

1 N. C. Chu, R. N. Taylor, V. Chavagnac, R. W. Nesbitt, R. M. Boella, J. A. Milton, C. R. German, G. Bayon and K. Burton, *J. Anal. At. Spectrom.*, 2002, **17**, 1567–1574.
2 W. L. Griffin, N. J. Pearson, E. Belousova, S. E. Jackson, E. van Achterbergh, S. Y. O'Reilly and S. R. Shee, *Geochim. Cosmochim. Acta*, 2000, **64**, 133–147.
3 J. Woodhead, J. Hergt, M. Shelley, S. Eggins and R. Kemp, *Chem. Geol.*, 2004, **209**, 121–135.
4 C. M. Fisher, J. M. Hanchar, S. D. Samson, B. Dhuime, J. Blichert-Toft, J. D. Vervoort and R. Lam, *Chem. Geol.*, 2011, **286**, 32–47.
5 N. J. Pearson, W. L. Griffin and S. Y. O'Reilly, in *Laser ablation-ICP-MS in the earth sciences: current practices and outstanding issues*, ed. P. Sylvester, Mineralogical Association of Canada, 2008, Short course series, vol. 40, pp. 93–116.
6 A. I. S. Kemp, G. L. Foster, A. Schersten, M. J. Whitehouse, J. Darling and C. Storey, *Chem. Geol.*, 2009, **261**, 244–260.

7 Y. Amelin and W. J. Davis, *Geochim. Cosmochim. Acta*, 2005, **69**, 465–473.
8 I. Segal, L. Halicz and I. T. Platzner, *J. Anal. At. Spectrom.*, 2003, **18**, 1217–1223.
9 M. R. Cecil, G. Gehrels, M. N. Ducea and P. J. Patchett, *Lithosphere*, 2011, **3**, 247–260.
10 C. J. Hawkesworth and A. I. S. Kemp, *Chem. Geol.*, 2006, **226**, 144–162.
11 H. S. C. O'Neill, *Am. Mineral.*, 2005, **90**, 497–501.
12 K. J. Grant and B. J. Wood, *Geochim. Cosmochim. Acta*, 2010, **74**, 2412–2428.
13 J. D. Vervoort, P. J. Patchett, U. Soderlund and M. Baker, *Geochem., Geophys., Geosyst.*, 2004, **5**, Q11002.
14 P. J. Patchett, O. Kouvo, C. E. Hedge and M. Tatsumoto, *Contrib. Mineral. Petrol.*, 1981, **78**, 279–297.
15 W. L. Griffin, X. Wang, S. E. Jackson, N. J. Pearson, S. Y. O'Reilly, X. S. Xu and X. M. Zhou, *Lithos*, 2002, **61**, 237–269.
16 J. BlichertToft, C. Chauvel and F. Albarede, *Contrib. Mineral. Petrol.*, 1997, **127**, 248–260.
17 K. R. Ludwig, *User's Manual for Isoplot 3.00*, 2003.
18 F. A. Macdonald, M. D. Schmitz, J. L. Crowley, C. F. Roots, D. S. Jones, A. C. Maloof, J. V. Strauss, P. A. Cohen, D. T. Johnston and D. P. Schrag, *Science*, 2010, **327**, 1241–1243.
19 A. J. R. Kent and C. A. Ungerer, *J. Anal. At. Spectrom.*, 2005, **20**, 1256–1262.
20 K. Newman, P. A. Freedman, J. Williams, N. S. Belshaw and A. N. Halliday, *J. Anal. At. Spectrom.*, 2009, **24**, 742–751.
21 E. A. Belousova, W. L. Griffin, S. Y. O'Reilly and N. I. Fisher, *Contrib. Mineral. Petrol.*, 2002, **143**, 602–622.
22 F. Y. Wu, Y. H. Yang, L. W. Xie, J. H. Yang and P. Xu, *Chem. Geol.*, 2006, **234**, 105–126.
23 W. V. Boynton, in *Rare Earth Element Geochemistry*, ed. P. Henderson, Elsevier, Amsterdam, 1984, pp. 63–114.